Materials Research Bulletin 110 (2019) 13–17

Contents lists available at ScienceDirect

Materials Research Bulletin

journal homepage: www.elsevier.com/locate/matresbu

# Experimental and first principle study of room temperature ferromagnetism in carbon-doped rutile $TiO_2$

Homnath Luitel[a,b], P. Chettri[c], A. Tiwari[c], D. Sanyal[a,b,*]

[a] Homi Bhabha National Institute, Training School Complex, Anushakti Nagar, Mumbai, 400094, India
[b] Variable Energy Cyclotron Centre, 1/AF Bidhannagar, Kolkata, 700064, India
[c] Department of Physics, School of Physical Sciences, Sikkim University, Gangtok, 737102, India

ARTICLE INFO

*Keywords:*
A. Semiconductors
B. Magnetic properties
D. Defects

ABSTRACT

Room temperature ferromagnetism has been observed experimentally by implanting 1.2 MeV carbon on rutile $TiO_2$. Density functional theory has been employed to study the magnetic properties of different possible carbon-related defects in $TiO_2$. Theoretical calculation suggests carbon-doped at oxygen site ($C_O$) can induce a significant magnetic moment in rutile $TiO_2$. The 2p orbital electrons of the carbon atom are the primary source of the induced magnetic moment in $TiO_2$. The magnetic measurements using a SQUID magnetometer, at room temperature, confirmed the ferromagnetic behavior of carbon doped rutile $TiO_2$ sample.

## 1. Introduction

The discovery of ferromagnetism in transition metals (Fe, Mn, Co, etc.,) doped semiconductors have opened a new frontier of research in condensed matter physics and materials science [1]. Ferromagnetism in semiconductors above room temperature is an essential requirement for spintronics application [2]. The ferromagnetic semiconductor could help the retention of memory within the semiconductor and thus a non-volatile transistor can be realized [2] along with the transport of spin-polarized electrons [3]. There are many experimental reports [4–8] of room temperature ferromagnetism in transition metal doped (< 4 at. %) ZnO and other non-magnetic oxides. However, the source of magnetism was debatable, since there are reports of room temperature ferromagnetism in these non-magnetic nanocrystalline oxides [9,10] even without any transition metal doping. Venkatesan et al. [11], reported ferromagnetism in the thin films of $HfO_2$ without any doping. Creating atomic defects in various nonmagnetic oxides (viz., ZnO, MgO, $SnO_2$, $TiO_2$, etc.,) stable ferromagnetism could be generated [12–21].

$TiO_2$ is a wide band gap semiconductor with a band gap of ~3 eV at room temperature [22]. This band gap makes it possible to absorb the UV radiation. The introduction of impurities creates new states above the valence band [23] which eventually reduces the band gap of the system and absorbs the visible band of the spectrum [24]. In recent years, $TiO_2$ based dilute magnetic semiconductors have drawn considerable research attention due to their potential application in optoelectronic, magneto-optic and spintronics devices [25,26]. Reports suggest that both cation [27] and anion vacancies [21] are responsible for inducing ferromagnetism in rutile $TiO_2$. Theoretical calculations indicate the possibility of the induced magnetic moment by substitution of carbon [28] and nitrogen [29] doped in anatase $TiO_2$. A detailed theoretical investigation for nitrogen doped anatase $TiO_2$ was carried out by Bai et al. [30]. The magnetic moment generated due to nitrogen doping in the anatase $TiO_2$ tend to couple anti-ferromagnetically and thus do not yield a significant moment in the system [30]. However, both theoretical and experimental investigations show room temperature ferromagnetism in nitrogen-doped rutile $TiO_2$ system [31,32]. Despite all these studies, the possibility of ferromagnetism in carbon-doped rutile $TiO_2$ is still unclear and needs further investigations taking into account the effect of atomic vacancies into the system.

In the present work, an *ab-initio* calculation using density functional theory has been carried out by considering all possibilities, which can generate a magnetic moment in rutile $TiO_2$. Intrinsic defects such as oxygen vacancies, metal vacancies, metal interstitials, the formation of $Ti^{3+}$, etc., are formed in the $TiO_2$ system [23]. Carbon-doped rutile $TiO_2$ system with various possible defect configurations, including atomic vacancies and dopant, has been considered for the present theoretical simulations. Further, the room temperature magnetic property of 1.2 MeV $C^{4+}$ ions irradiated/implanted rutile $TiO_2$ sample has been experimentally measured.

* Corresponding author at: Homi Bhabha National Institute, Training School Complex, Anushakti Nagar, Mumbai, 400094, India.
*E-mail address:* dirtha@vecc.gov.in (D. Sanyal).

https://doi.org/10.1016/j.materresbull.2018.10.004
Received 1 June 2018; Received in revised form 18 September 2018; Accepted 2 October 2018
Available online 04 October 2018
0025-5408/ 

## 2. Experimental outline

Pellets (thickness ~0.5 mm) of rutile-$TiO_2$ with 99.998% purity (Alfa Aesar, Johnson Mathey, Germany) have been made by applying a constant pressure of ~ 220 MPa followed by annealing at 500 °C for 5 h. Afterward, the annealed pellets were irradiated uniformly by 1.2 MeV $C^{4+}$ ion beam, available from the VECC radioactive ion beam (RIB) facility [33–35]. A total fluence of $1 \times 10^{16}$ ions/cm$^2$ with a constant beam current of 1.5 μA has been used to have about 1% doping. The magnetic measurements have been carried out using the squid magnetometer (Quantum Design, MPMS-3).

## 3. Computational methodology

Density functional theory (DFT) has been employed for the theoretical calculations using MedeA software package, based on Vienna *ab-initio* simulation (VASP) code [36–39]. A supercell of rutile $TiO_2$ (a = b = 4.59 Å and c = 2.96 Å, α = β = γ = 90°) with 72 atoms (2 × 2 × 3 unit cells) has structurally optimized. The magnetic calculations are carried out in the optimized supercell. Generalized gradient approximation (GGA) with Perdew-Burke-Ernzerhof (PBE) exchange and correlation [40] method and PAW pseudo-potentials have been used in all the calculations. Periodic boundary conditions have been implemented to the basis vectors. Systematic substitution of single Ti/O atom is carried out with C atom in various configuration (i.e., $Ti_{24-m}C_{m+n}O_{48-n}$, n and m are integers), in the $TiO_2$ super-cell. Several $TiO_2$ systems with the following defect combinations e.g., C-doped at O-site ($C_O$); C-doped at O-site plus one oxygen vacancy at the vicinity of $C_O$ ($C_O + V_O$); C-doped at O-site plus two oxygen vacancies at the vicinity of $C_O$ ($C_O + 2V_O\_S$); C-doped at O-site plus two oxygen vacancies (one at vicinity of $C_O$ and the other in the next unit cell) ($C_O + 2V_O\_F$); C-doped at Ti-site plus one oxygen vacancy at the vicinity $C_O$ ($C_{Ti} + V_O$); C-doped at interstitial site ($C_i$); and C-doped at O-site along with a carbon at interstitial position and one oxygen vacancy ($C_O + V_O + C_i$), have been constructed. The optimization of each structure has been carried out by geometrically relaxing the atomic positions until the maximum value of Hellman-Feynman force is less than 0.02 eV/Å. A tolerance of $10^{-5}$ eV (as the stopping criteria) has been fixed for the self-consistent loop to reach the electronic ground state. Similarly to expand the plane wave basis set, 400 eV mesh cut-off energy is fixed in all the calculations. For each optimized structure, the density of states (spin-polarized) has been calculated. The 3 × 3 × 3 Monkhorst-Pack (MP) k-points [41] have been utilized to divide the Brillouin zone of the supercell. The spin-spin interaction study for determining the minimum energy (free energy) in between the parallel (spin-triplet) and anti-parallel (spin-singlet) state has been carried out. Spins of all the atoms have aligned in one direction to make the system ferromagnetic. Whereas, the G-type anti-ferromagnetism is obtained by assigning opposite spins to the two carbon atoms doped at O-sites and also assigning opposite spins to the nearby Ti and O atoms present in the system.

The energy loss profile, the carbon ions distribution profile and the atomic vacancies generation during 1.2 MeV $C^{4+}$ ions irradiation on $TiO_2$ have been simulated using SRIM and TRIM packages [42].

## 4. Results and discussion

Magnetic properties of carbon-doped rutile $TiO_2$ system have been studied using first principle calculation. The doping of carbon atom at an oxygen site generates a significant amount of magnetic moment. Carbon atom ($1s^2$, $2s^2$, $2p^2$) when doped at O-site gets two electrons from nearby Ti-atoms and becomes $2s^2$, $2p^4$ in the valence shell. As a result, carbon atom contributes ~2$\mu_B$ magnetic moment in the $TiO_2$ system. The oxygen atoms present in the neighboring site makes a small contribution in net magnetization due to the effect of polarization. Presence of different vacancies inside the undoped $TiO_2$ system mainly generates the magnetic moment in $TiO_2$. The value of the magnetic moment induced in the $TiO_2$ with different configurations has been tabulated in Table 1.

**Table 1**
The defect formation energy, induced magnetic moment, Fermi energy and Fermi energy shift with respect to pristine TiO2 for different defect configurations created in rutile TiO2.

| $TiO_2$ System | Defect Formation Energy (eV) | Induced Magnetic Moment ($\mu_B$) | Fermi Energy (eV) | Fermi Energy shift (eV) |
|---|---|---|---|---|
| $C_O$ ($Ti_{24}CO_{47}$) | 4.04 | 2.27 | 5.78 | 2.35 |
| $C_O + V_O$ ($Ti_{23}NO_{46}$) | 11.14 | 0.09 | 5.41 | 1.98 |
| $C_{Ti} + V_O$ ($Ti_{23}$ $CO_{47}$) | 14.47 | 0.00 | 5.19 | 1.76 |
| $C_i$($Ti_{24}CO_{48}$) | −4.13 | 0.03 | 7.12 | 3.69 |
| $C_O + 2V_O\_N$($Ti_{24}CO_{45}$) | 20.53 | 0.32 | 6.87 | 3.44 |
| $C_O + 2V_O\_F$ ($Ti_{24}CO_{45}$) | 20.86 | 0.83 | 6.88 | 3.45 |
| $C_i + C_O + V_O$ ($Ti_{24}C_2O_{46}$) | 5.92 | 0.07 | 7.04 | 3.62 |

Doping of one carbon atom at oxygen site generates about 2.2$\mu_B$ magnetic moment. The magnetic moment generated from the 2p orbital of carbon atom polarizes the 3d-orbital of nearby Ti-atoms, which causes the ferromagnetic interactions in the C-doped $TiO_2$ system. The magnetic moment in the carbon-doped rutile $TiO_2$ system favors parallel spin alignment as the ground state energy for the ferromagnetic state is 88 meV less as compared to the anti-ferromagnetic state. The 2p-orbital electrons of the doped carbon atom are the primary source of magnetism, a small contribution of the magnetic moment comes from neighboring oxygen atoms. Presence of one oxygen vacancy attached to carbon atom reduces the magnetic moment significantly (as in the case of $C_O + V_O$). Adding one more oxygen vacancy near the carbon atom, i.e., in case of $C_O + 2V_O\_S$, the total magnetic moment of the system slightly increases. The increase comes from the contribution of 3d-orbital electrons of Ti atoms surrounding the vacancies. Changing the position of the second oxygen vacancy in the $TiO_2$ matrix ($C_O + 2V_O\_F$) further increases of the magnetic moment has been observed. The additional contribution comes from the effect of a single oxygen vacancy. The creation of oxygen vacancy induces a significant magnetism in $TiO_2$ [21]. The presence of another oxygen vacancy enhances the magnetic moment generated due to the substitution of carbon at the oxygen site. Doping of carbon atom at titanium site does not induce any magnetic moment in the system. Removal of an oxygen atom attached to carbon atom doped at Ti-site also does not contribute any moment. The incorporation of a nitrogen atom in the interstitial site generates a significant moment in $TiO_2$ [32], but carbon doped at the interstitial position does not show any change in the magnetic moment of the system. Also, no significant magnetic moment has been observed for carbon doped at the interstitial position together with other configuration in the $TiO_2$ system e.g., ($C_i + C_O + V_O$). The differential charge distribution in carbon-doped $TiO_2$ is shown in Fig. 1. The Bader charge analysis for carbon-doped $TiO_2$ system shows that carbon atom is negatively charged at the lattice. The carbon atom placed at the oxygen site has a total valence charge of 4.78e with charge transfer of - 0.78e. The obtained values of the charge transfer in Ti-atom and O-atom in the carbon-doped $TiO_2$ system are +2.22e and -1.12e respectively, which indicates that the carbon atom can be substituted at the oxygen site, as both are showing the same chemical behavior when doped at $TiO_2$ system.

The values of defect formation energy ($E_{df}$), Fermi energy and the Fermi energy shift with respect to the pristine $TiO_2$ has shown in Table 1. The formula for the calculation of the defect formation energy, $E_{df}$ is represented by the following equation [17,43]

$$E_{df} = E(\mathrm{Ti_{24\text{-}m}C_{m+n}O_{48\text{-}n}}) - E(Ti_{12}O_{24})_2 + nE(O) + mE(Ti) - (m+n)E(C) \quad (1)$$

where, $E(Ti_{24}O_{48})$ represents the total energy of the pristine system and $E(Ti_{24\text{-}m}C_{m+n}O_{48\text{-}n})$ is the total energy of the defect bearing system.

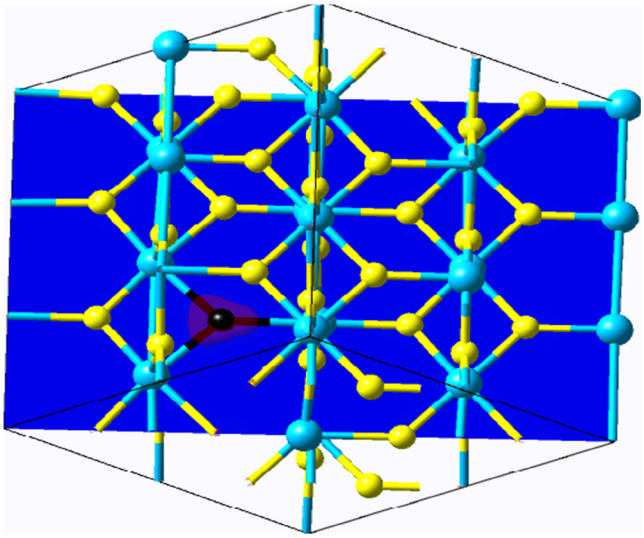

**Fig. 1.** Differential charge distribution in carbon-doped $TiO_2$ system. The Black sphere ball represents the carbon atom substituted at O-site.

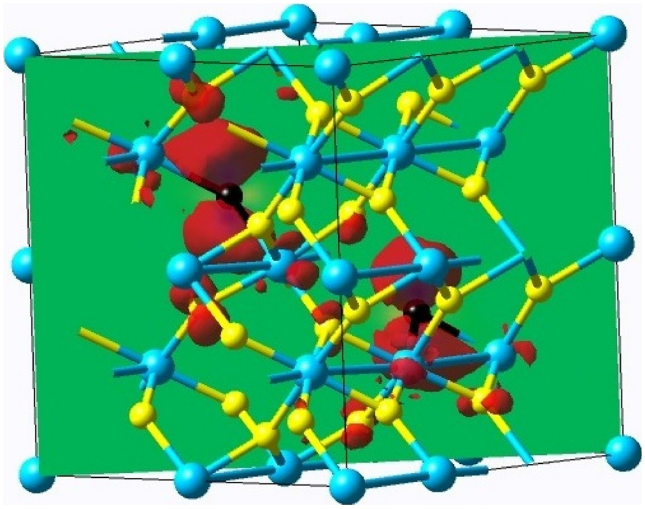

**Fig. 3.** Magnetization density (spin-polarized) distribution in $TiO_2$ with $C_O$. The blue, yellow and black color spheres are Ti-atoms, O-atoms and C-atoms respectively. The red color cloud-like structure represents the localized magnetization density distribution (For interpretation of the references to colour in this figure legend, the reader is referred to the web version of this article).

Similarly, *E(O), E(Ti),* and *E(C)* are the free energy value of a single oxygen atom, a titanium atom and a carbon atom respectively.

It has observed from the Table 1 that the defect formation energy of the $TiO_2$ with carbon-doped at oxygen site is only about 4 eV, which makes the system viable. The spin-polarized density of states for pristine $TiO_2$, $TiO_2$ with interstitial carbon and $TiO_2$ with $C_O$ (carbon at oxygen site) have shown in Fig. 2(a)–(c) respectively. The spin-polarized density of states for pristine $TiO_2$ shows a symmetric density of states in both up and down spin direction, resulting a net zero electron spin DOS and hence a zero magnetic moment. But, the total density of states for the carbon-doped $TiO_2$ has been depicted in Fig. 2(c) is asymmetric. This is due to the 2p orbital electron of carbon, along with 3d orbital electron of Ti-atom and 2p-orbital electron of oxygen-atom. As a result, the system shows a non-zero value in the magnetic moment. Similarly, in case of $TiO_2$ with a carbon atom at the interstitial site, the 2p orbital electron of carbon has an asymmetric partial density of states, but it has minimal effect in the total density of states and yields no net magnetism in the system.

The magnetization density (spin-polarized) distribution has been plotted in Fig. 3. It can be observed from the Fig. 3 that magnetic density is mainly localized around the dopant atom and a small fraction is present around the neighboring oxygen atoms. Thus, the result of local magnetic density distribution supports the result obtained from the density of states (DOS) for all the studied cases. Both calculations indicate the carbon atom as the source of magnetism in the carbon-doped $TiO_2$ system. The doping of carbon in $TiO_2$ introduces some new states above valence band leading to the shift in the Fermi level in all cases. Typically, the sheet resistance of $TiO_2$ is about $10^7\ \Omega\ cm^{-2}$ [21]. Earlier, we have seen that due to $V_O$ the sheet resistance decreases to $3 \times 10^3\ \Omega\ cm^{-2}$ [21]. Thus, a decrease of sheet resistance is a measure of n-type semi-conductivity; otherwise, it will be p-type. In the present case, we observed the sheet resistance decreases almost the same order ($10^3\ \Omega\ cm^{-2}$) due to carbon irradiation, which confirms the n-type semi-conductivity in the irradiated sample.

Fig. 4(a) represents the energy loss profile for the carbon ion irradiated $TiO_2$ using SRIM software. From the SRIM simulation, it has been found that the nuclear energy loss is dominant up to 17 keV, whereas the electronic energy loss and the nuclear energy loss at 1.2 MeV $C^{4+}$ ions on $TiO_2$ have been found to be 131.0 eV/Å and 1.0 eV/Å respectively. Atomic vacancies in a system are generated by the nuclear energy loss mechanism of the irradiated ions [44]. As a result, fewer atomic vacancies are generated at the surface of the sample for 1.2 MeV

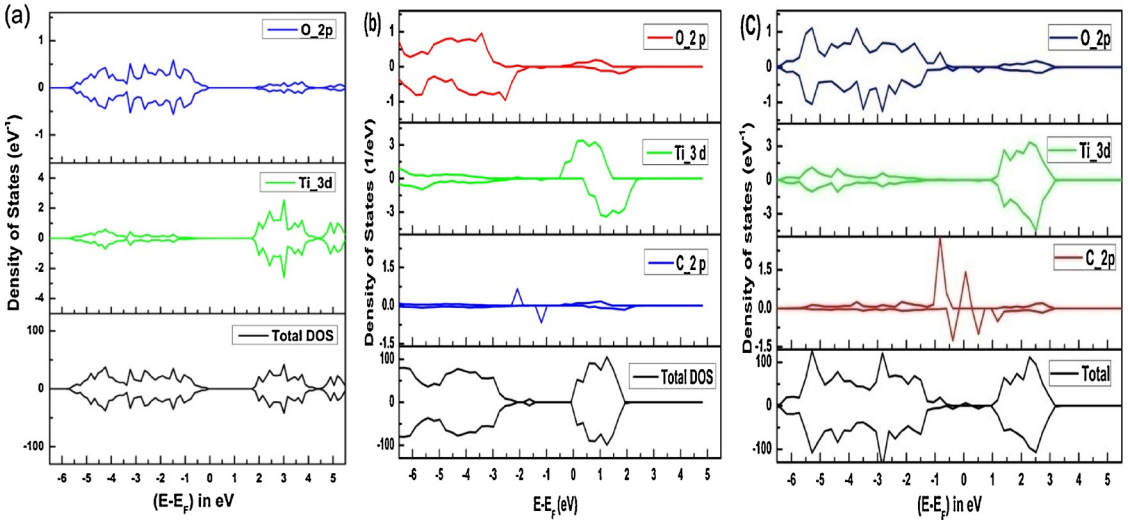


**Fig. 2.** Spin-polarized DOS for (a) pristine $TiO_2$, (b) $TiO_2$ with $C_i$, (c) $TiO_2$ with $C_O$.

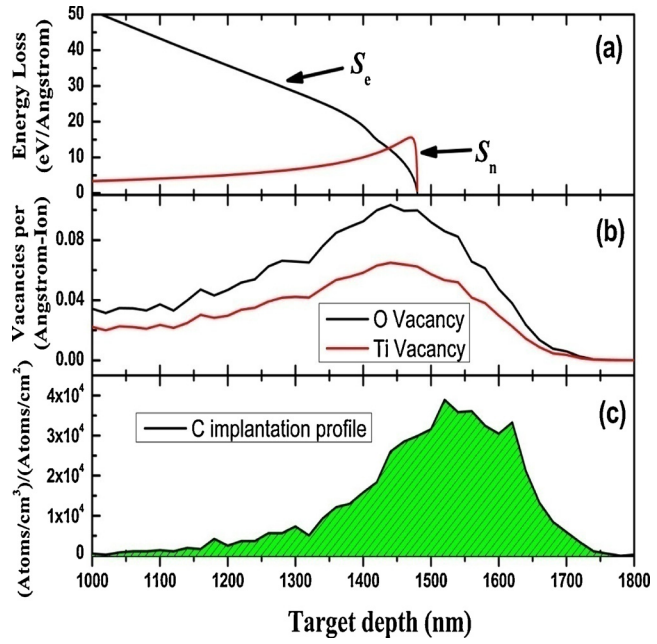


**Fig. 4.** SRIM simulation for $C^{4+}$ irradiated $TiO_2$ (a) energy loss profile, (b) vacancy formation profile and (c) distribution of carbon ions with target depth. $S_n$ and $S_e$ represent nuclear energy loss and electronic energy loss respectively.

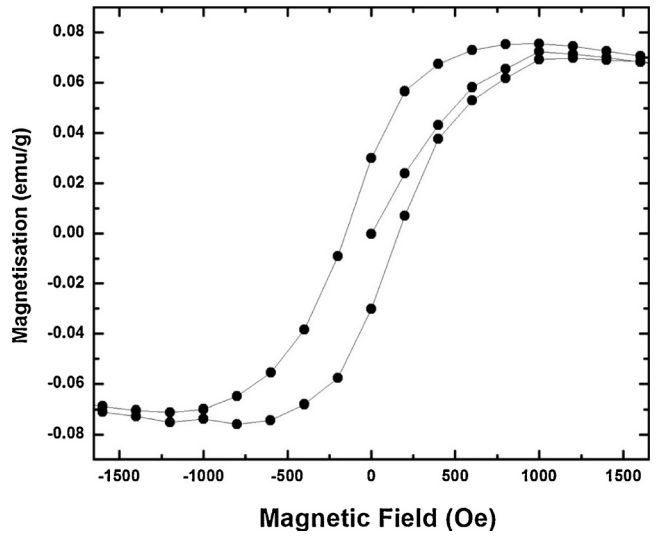


**Fig. 5.** Magnetization (M) vs. Field (H) graph for 1.2 MeV carbon implanted rutile $TiO_2$.

$C^{4+}$ ions and it increases with the depth of the sample due to the decrease in energy of irradiated ions. This behavior was also verified utilizing TRIM simulation and shown in Fig. 4(b). From the vacancy profile in Fig. 4(b), it has been observed that both $V_{Ti}$ and $V_O$ have been created in $TiO_2$ when irradiated with 1.2 MeV $C^{4+}$ ions, but the number of oxygen vacancies generated is more in comparison to titanium vacancies. Fig. 4(c) depicts the distribution of carbon ions with the depth of the sample. From this Figure, it is also observed that the 1.2 MeV carbon ions can penetrate up to a depth of 1.78 μm and the maximum ion distribution occurs at a depth of 1.52 μm in the polycrystalline $TiO_2$ sample. The variation of Magnetization (M) with Field (H) for the $C^{4+}$ irradiated $TiO_2$ sample is represented in Fig. 5. The M vs. H curve represents a significant hysteresis loop at room temperature (~300 K). From the hysteresis curve, the value of saturation magnetization ($M_s$) and coercive field ($H_C$) has been found to be $7.5 \times 10^{-2}$ emu/g and 156 Oe respectively. The magnetization (M) recorded in the present case is higher than the earlier reported experimental value with oxygen vacancies created due to Ar ions irradiation (~ $4 \times 10^{-4}$ emu/g [21]) and annealing at $H_2$/Ar atmosphere (~ $8 \times 10^{-3}$ emu/g [45]). The higher value of saturation magnetization in $C^{4+}$ ion irradiated rutile $TiO_2$ is possibly due to the additional contributions of magnetism from carbon atoms at $C_O$ site. The effective magnetic moment per dopant has been calculated to be ~ 1.5 $\mu_B$ per dopant, which is little less as compared to the theoretical value of 2 $\mu_B$, this may be, a part of implanted carbon is going to the interstitial position. The carbon atoms placed at interstitials site do not contribute in the effective moment. The hysteresis curve as obtained from the present experimental data at room temperature (300 K) suggests the presence of room temperature ferromagnetism in 1.2 MeV carbon ions implanted rutile $TiO_2$.

## 5. Conclusions

The first principle calculations based on density functional theory predicts the possibility of ferromagnetism in carbon-doped rutile $TiO_2$ system. The 2p-orbital electrons of dopant along with small contributions from oxygen atoms present nearby the dopant are the source of induced magnetism in the system. The irradiation of carbon ions creates a large number of atomic vacancies. The presence of oxygen vacancies in the vicinity of dopant does not induce any magnetic moment. However, the creation of oxygen vacancy far from the dopant contribute magnetism and enhances the net magnetic moment in the carbon-doped $TiO_2$ system. The theoretical calculations are supported by experimental observations. Magnetic measurement at room temperature (300 K) shows ferromagnetic behavior in 1.2 MeV $C^{4+}$ ions irradiated/implanted rutile $TiO_2$ sample.

## Acknowledgements

One of the authors (H. Luitel) is thankful to Department of Atomic Energy, Government of India (DAE) for financial support as a Senior Research Fellow (SRF) to carry out the research work at Variable Energy Cyclotron Centre, Kolkata. PC thanks Department of Science and Technology, Government of India (No: DST/INSPIRE Fellowship/2013/958) [IF130752] for financial support under DST INSPIRE scheme.

## References

[1] T. Dietl, H. Ohno, F.M. Atsukura, J. Cibert, D. Ferrand, Zener model description of ferromagnetism in zinc-blende magnetic semiconductors, Science 287 (2000) 1019–1022.
[2] K. Ando, Seeking room temperature ferromagnetic semiconductor, Science 312 (2006) 1883–1885.
[3] T. Dietl, A ten-year perspective on dilute magnetic semiconductors and oxides, Nat. Mater. 9 (2010) 965–974.
[4] P. Sharma, A. Gupta, K.V. Rao, J.O. Frank, R. Sharma, R. Ahuja, J.M.O. Guillen, B. Johansson, G.A. Gehring, Ferromagnetism above room temperature in bulk and transparent thin films of Mn-doped ZnO, Nat. Mater. 2 (2003) 673–677.
[5] K. Ueda, H. Tabata, T. Kawai, Magnetic and electric properties of transition-metal-doped ZnO films, Appl. Phys. Lett. 79 (2001) 988.
[6] A. Punnoose, J. Hays, A. Thurber, M.H. Engelhard, R.K. Kukkadapu, C. Wang, V. Shuttanandan, S. Thevuthasan, Development of high-temperature ferromagnetism in $SnO_2$ and paramagnetism in SnO by Fe doping, Phys. Rev. B 72 (2005) 054402.
[7] J. Hays, A. Punnoose, R. Baldner, M.H. Engelhard, J. Peloquin, K.M. Reddy, Relationship between the structural and magnetic properties of Co-doped nanoparticles, Phys. Rev. B 72 (2005) 075203.
[8] R.K. Kittilstved, N.S. Norberg, D.R. Gamelin, Chemical manipulation of high-$T_c$ ferromagnetism in ZnO diluted magnetic semiconductor, Phys. Rev. Lett. 94 (2005) 147209.
[9] A. Sundaresan, R. Bhargavi, N. Rangarajan, U. Siddesh, C.N.R. Rao, Ferromagnetism as a universal feature of nanoparticles of the otherwise non-magnetic oxides, Phys. Rev. B 74 (2006) 16106 (R).
[10] D. Sanyal, M. Chakrabarti, T.K. Roy, A. Chakrabarti, The origin of ferromagnetism and defect-magnetism correlation in nanocrystalline ZnO, Phys. Lett. A 371 (2007) 482–485.
[11] M. Venkatesan, C.B. Fitzgerald, J.M.D. Coey, Unexpected magnetism in a dielectric oxide, Nat. Commun. 430 (2004) 630.
[12] H. Pan, J.B. Yi, L. Shen, R.Q. Wu, J.H. Yang, J.P. Feng, J. Ding, L.H. Van, J.H. Yin, Room-temperature ferromagnetism in carbon-doped ZnO, Phys. Rev. Lett. 99

(2007) 127201.
[13] H. Peng, J. Li, S.S. Li, J.B. Xia, Possible origin of ferromagnetism in undoped anatase $TiO_2$, Phys. Rev. B 79 (2009) 092411.
[14] H. Luitel, S. Roy, D. Sanyal, Ab-initio calculation of magnetic properties of P and As doped $SnO_2$, Comput. Cond. Matter 14 (2018) 36–39.
[15] H. Luitel, D. Sanyal, *Ab-initio* calculation of magnetic properties in B, Al, C, Si, N, P and As doped rutile $TiO_2$, Int. J. Mod. Phys. B 31 (2017) 1750227.
[16] L. Shen, R.Q. Wu, H. Pan, G.W. Peng, M. Yang, Z.D. Sha, Y.P. Feng, Mechanism of ferromagnetism in nitrogen-doped ZnO: first-principle calculations, Phys. Rev. B 78 (2008) 073306.
[17] P. Nath, A. Chakraborty, D. Sanyal, *Ab initio* calculation of magnetic properties of p-block element doped ZnO, RSC Adv. 4 (2014) 45598–45602.
[18] A. Sarkar, D. Sanyal, P. Nath, M. Chakrabarti, S. Pal, S. Chattopadhyay, D. Jana, K. Asokan, Defect driven ferromagnetism in $SnO_2$: a combined density functional theory and positron annihilation spectroscopy, RSC Adv. 5 (2015) 1148–1152.
[19] N. Kumar, D. Sanyal, A. Sundaresan, Defect induced Ferromagnetism in MgO nanoparticles studied by optical and positron annihilation spectroscopy, Chem. Phys. Lett. 477 (2009) 360–364.
[20] S. Wang, L. Pan, J.J. Song, W. Mi, J.J. Zou, L. Wang, X. Zhang, Titanium-defected undoped anatase $TiO_2$ with p-type conductivity, room temperature ferromagnetism and remarkable photocatalytic performance, J. Am. Chem. Soc. 137 (2015) 2975–2983.
[21] D. Sanyal, M. Chakrabarti, P. Nath, A. Sarkar, D. Bhowmick, A. Chakrabarti, Room temperature ferromagnetic ordering in 4 MeV $Ar^{5+}$ irradiated $TiO_2$, J. Phys. D Appl. Phys. 47 (2014) 025001.
[22] J. Pascual, J. Camassel, H. Mathieu, Fine structure in the intrinsic absorption edge of $TiO_2$, Phys. Rev. B 18 (1978) 5606–5614.
[23] J. Navas, A.S. Coronilla, T. Aguilar, C.N. Hernandez, D.M. de los Santos, J.S. Marquez, D. Zorrilla, C.F. Lorenzo, R. Alcantara, J.M. Calleja, Experimental and theoretical study of the electronic properties of Cu-doped anatase $TiO_2$, Phys. Chem. Chem. Phys. 16 (2014) 3835–3845.
[24] B. Choudhury, M. Dey, A. Choudhury, Defect generation, d-d transition, and band gap reduction in Cu-doped $TiO_2$ nanoparticles, Int. Nano Lett 3 (2013) 25.
[25] H. Ohno, Towards functional spintronics, Science 291 (2001) 840–841.
[26] S.A. Wolf, D.D. Awschalom, R.A. Buhrman, J.M. Daughton, S.V. Molnar, M.L. Roukes, A.Y. Chtchelkanova, D.M. Treger, Spintronics: a spin-based electronics vision for the future, Science 294 (2001) 1488–1495.
[27] H. Luitel, A. Sarkar, M. Chakrabarti, S. Chattopadhyay, K. Asokan, D. Sanyal, Positron annihilation lifetime characterization of oxygen ion irradiated rutile $TiO_2$, Nucl. Inst. Method 379 (2016) 215–218.
[28] K. Yang, Y. Dai, B. Huang, M.H. Whangbo, On the possibility of ferromagnetism in carbon-doped anatase $TiO_2$, Appl. Phys. Lett. 93 (2008) 132507.
[29] J.G. Tao, L.X. Guan, J.S. Pan, C.H.A. Huan, L. Wang, J. Zhang, J.W. Chai, S.J. Wang, Density functional study on ferromagnetism in nitrogen doped anatase $TiO_2$, Appl. Phys. Lett. 95 (2009) 062505.
[30] Y. Bai, Q. Chen, N-dopant induced antiferromagnetism in anatase $TiO_2$: first principle study, Solide State Commun. 147 (2008) 169–171.
[31] K. Yang, Y. Dai, B. Huang, M.H. Whangbo, Density functional studies of the magnetic properties in nitrogen doped $TiO_2$, Chem. Phys. Lett. 481 (2009) 99–102.
[32] H. Luitel, M. Chakrabarti, A. Sarkar, S. Dechoudhury, D. Bhowmick, V. Naik, D. Sanyal, Ab-initio calculation and experimental observation of room temperature ferromagnetism in 50 keV nitrogen implanted rutile $TiO_2$, Mat. Res. Exp. 5 (2018) 026104.
[33] A. Chakrabarti, The radioactive ion beam project at VECC, Kolkata- A status report, Paramana 59 (2002) 923–932.
[34] A. Chakrabarti, A. Bandyopadhyay, V. Naik, S. Dechoudhury, M. Mondal, P.Y. Nabhiraj, The ANURIB project at VECC-Plans and preparations, Nucl. Inst. Method 317 (2013) 253–256.
[35] S. Dechoudhury, V. Naik, M. Mondal, A. Chatterjee, H.K. Pandey, T.K. Mandi, A. Bandyopadhyay, P. Karmakar, S. Bhattacharjee, P.S. Chouhan, S. Ali, S.C.L. Srivastava, A. Chakrabarti, Design and development of radio frequency quardrupole linac post-accelerator for the Variable Energy Cyclotron Centre rare ion beam project, Rev. Sci. Instrum. 81 (2010) 023301.
[36] G. Kresse, J. Hafner, *Ab initio* molecular dynamics for liquid metals, Phys. Rev. B 47 (1993) 558–561.
[37] G. Kresse, J. Hafner, Ab-initio molecular-dynamics simulation of the liquid-metal-amorphous-semiconductor transition in germanium, Phys. Rev. B 49 (1994) 14251–14271.
[38] G. Kresse, J. Furthmüller, Efficiency of *ab-initio* total energy calculations for metals and semiconductors using a plane-wave basis set, Comput. Mater. Sci. 6 (1996) 15–50.
[39] G. Kresse, J. Furthmüller, Efficient iterative schemes for ab-initio total-energy calculations using a plane-wave basis set, Phys. Rev. B 54 (1996) 11169–11186.
[40] J.P. Perdew, K. Burke, M. Ernzerhof, Generalized gradient approximation made simple, Phys. Rev. Lett. 77 (1996) 3865–3868.
[41] H.J. Monkhorst, J.D. Pack, Special points for Brillouin-zone integrations, Phys. Rev. B 13 (1976) 5188–5192.
[42] J. Ziegler, J. Biersack, U. Littmark, The Stopping and Range of Ions in Matter, SRIM 2008 code Pergamon, New York, 1985www.srim.org.
[43] N. Seriani, C. Pinilla, Y. Crespo, Presence of gap states at Cu/$TiO_2$ anatase surfaces: consequences for the photocatalytic activity, J. Phys. Chem. C 119 (2015) 6696–6702.
[44] A.V. Krasheninnikov, K. Nordlund, Ion and electron irradiation-induced effects in nanostructured materials, J. Appl. Phys. 107 (2010) 071301.
[45] Z. Qian, W.U. Ping, L.I. Bao-ling, L.U. Zan-Ming, J. En-Yong, Room temperature ferromagnetism in semiconducting $TiO_{2-\delta}$ nanoparticles, Chin. Phys. Lett 25 (2008) 1811–1814.